Strong Charge-Transfer Doping of 1 to 10 Layer Graphene by NO_2

Andrew C. Crowther,* Amanda Ghassaei, Naeyoung Jung, and Louis E. Brus

Department of Chemistry, Columbia University, New York, New York 10027, United States

ABSTRACT

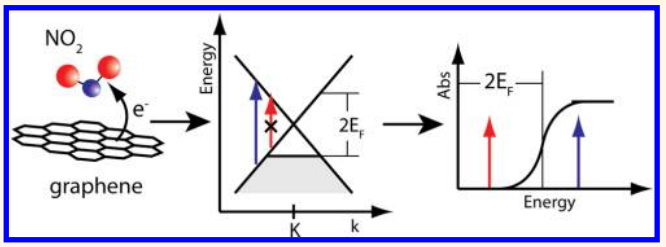

We use resonance Raman and optical reflection contrast methods to study charge transfer in 1−10 layer (1L−10L) thick graphene samples on which NO_2 has adsorbed. Electrons transfer from the graphene to NO_2, leaving the graphene layers doped with mobile delocalized holes. Doping follows a Langmuir-type isotherm as a function of NO_2 pressure. Raman and optical contrast spectra provide independent, self-consistent measures of the hole density and distribution as a function of the number of layers (N). At high doping, as the Fermi level shift E_F reaches half the laser photon energy, a resonance in the graphene G mode Raman intensity is observed. We observe a decrease of graphene optical absorption in the near-IR that is due to hole-doping. Highly doped graphene is more optically transparent and much more electrically conductive than intrinsic graphene. In thicker samples, holes are effectively confined near the surface, and in these samples, a small band gap opens near the surface. We discuss the properties and versatility of these highly charge-transfer-doped, few-layer-thick graphene samples as a new class of electronic materials.

KEYWORDS: graphene · NO_2 · nitrogen dioxide · Raman spectroscopy · charge transfer · doping

Single-layer graphene is a very stable, nearly chemically inert aromatic carbon membrane. Its local properties, such as chemical reactivity, can be naturally understood as those of a large aromatic hydrocarbon molecule. Graphene also has delocalized solid state properties as a result of its infinite two-dimensional crystalline structure. As planar aromatic hydrocarbon molecules increase in size toward the graphene limit, the π electron HOMO−LUMO gap goes to zero. Thus graphene is a "semi-metallic" material in which delocalized π electrons at the vanishing gap (the intrinsic Fermi level) carry electrical current at room temperature. Pristine undoped graphene has a very low density of states at the Fermi level, due to graphene's unique band structure around the K point in the Brillouin zone.[1] As a consequence, graphene is an unusual metal whose Fermi level can be significantly shifted by adding or removing electrons; this differs dramatically from traditional metals such as Cu. The density of states at the Fermi level increases as charge is added or subtracted, increasing electrical conductivity.

Charge transfer onto graphene by adsorbed species can shift the Fermi level more than an electronvolt and increase the conductivity by orders of magnitude, without requiring an external power source.[2−4] This paper focuses on the fundamental electronic structure of such very highly doped graphenes. Precise chemical control of such charge transfer onto graphene is crucial for future graphene applications, solar cells and transparent electrodes being important examples. Charge-donating species can both adsorb on and intercalate between graphene layers.[3,5−7] Charge-transfer doping as has been studied for many years in bulk graphite intercalation compounds (GICs),[8] and calculations of graphene's electronic structure as a function of thickness show that the electronic bands of 10L graphene differ from graphite by less than 10%. (where L signifies a layer of graphene).[9] In this study, we use Raman and contrast spectroscopy to comprehensively study strong hole-doping of 1L to 10L graphene upon adsorption of NO_2.

The Raman spectra D, G, and 2D peaks are important, nondestructive markers of the structure and doping of graphene. The D peak at 1350 cm^{-1} is Raman-active only when there are instances of sp^3 hybridization in the graphene, so its absence indicates pristine graphene, while its presence indicates defects such as vacancies, edges, or out-of-plane chemical bonds. The in-plane Raman G peak at 1580 cm^{-1}, a doubly degenerate phonon mode at the Γ point, indicates the extent of charge transfer.

* Address correspondence to ac3163@columbia.edu.

Received for review January 17, 2012 and accepted January 25, 2012.

Published online 10.1021/nn300252a

As the Fermi level shifts, nonadiabatic electron–phonon coupling leads to stiffening of the G peak; this raises the energy of the phonon mode.[10−12] Previous electric field gating experiments in devices have quantified the relationship between the G peak shift and the Fermi level shift.[10,11,13,14] In addition, the G peak width decreases when the Fermi level shifts past $\hbar\omega_{ph}/2$ because the phonon can no longer decay into low-energy electron–hole pairs; this necessarily increases the phonon lifetime.[10−14] The double resonant 2D peak at 2650 cm^{-1} is a single, symmetric peak for 1L graphene, but it becomes progressively more structured as samples become thicker. This structure makes the 2D peak a valuable indicator for single-layer graphene. The 2D peak intensity also decreases as doping increases because electron–electron scattering becomes competitive with electron–phonon scattering.[15]

G mode Raman spectroscopy has been quite informative in the study of bulk GICs intercalated by electron dopants such as Cs, K, and Rb and hole-dopants such as Br_2, $FeCl_3$, $SbCl_5$, and $AlCl_3$.[7] GICs form with different "stages" as a function of the intercalant chemical potential. The stage indicates the number of graphene layers between each intercalant layer. For example, $FeCl_3$ experiments formed stages ranging from 1 to 11.[8] For stage 1 and 2, the Raman spectrum shows a single upshifted peak that reflects equal doping for each layer. For stage 3 and greater, the Raman spectrum splits into two peaks, a "less-doped" peak at 1580–1584 cm^{-1} assigned to interior layers and a "more-doped" peak at 1596 to 1602 cm^{-1} assigned to surface layers. The same trends occur for $SbCl_5$ and $AlCl_3$ GICs[16,17] and for iodine and sulfuric acid surface adsorption on 1L to 4L graphene.[5,18] Rao and co-workers doped 3–4-layer graphene generated from exfoliated graphitic oxide by taking advantage of the range of electron-withdrawing and electron-donating strengths of substituted benzene molecules.[19] For example, increasing the concentration of hole-doping nitrobenzne and electron-doping aniline generated greater G peak upshifts and downshifts, respectively. They also observed this trend for 3–5-layer graphene doped by tetrathiafulvalene (TTF, electron-doping) and tetracyanoethylene (TCNE, hole-doping) in solution, along with charge-transfer bands in the visible absorption spectra.[20,21]

Graphene exhibits an optical absorption spectrum that is flat and featureless, absorbing 2.3% per layer from the infrared through the visible,[22,23] gradually increasing with photon energy until reaching a Fano resonance peak at 4.6 eV. This resonance is due to an interband exciton at the M point saddle singularity.[24] In pristine graphene, the infrared and visible photons absorb *via* interband transitions between the π and π^* linear bands about the K point. We show this electronic band structure and the resulting absorption spectrum schematically in the top and bottom panels of Figure 1a, respectively. Charge-transfer-doped graphene will exhibit no interband absorption for energies less than twice the Fermi level shift ($2E_F$), so the cutoff (*i.e.*, bleach) in the absorption spectrum is a direct measurement of the Fermi level shift (Figure 1b).

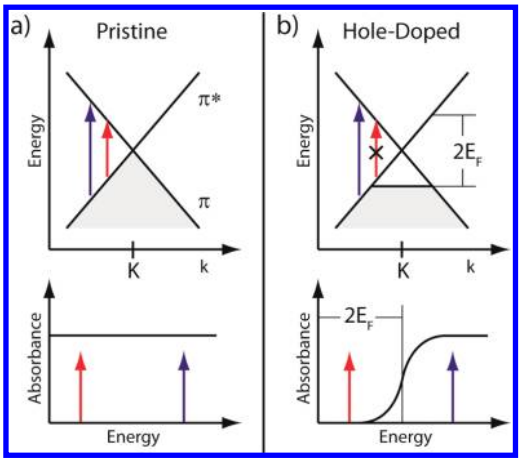

Figure 1. Schematic of electronic band structure and interband optical absorption for pristine (a) and hole-doped (b) graphene. The red and blue arrows represent absorption at low and high energies, respectively. (a) Pristine graphene has a flat interband absorption spectrum. (b) Hole-doped graphene shifts the Fermi level to lower energy by E_F. Hole-doped graphene does not absorb light below $2E_F$, as shown by the red arrows.

In this paper, we study the electronic and optical properties of graphene that is highly hole-doped due to electron transfer to NO_2. NO_2 is paramagnetic and has a high electron affinity (2.3 eV), and previous electrical measurements and theory show that at low NO_2 pressures there is full electron transfer from graphene to adsorbed NO_2 molecules.[25,26] Previous experimental studies have taken advantage of the strong electron transfer between NO_2 and graphene to investigate graphene's feasability as a chemical sensor.[25,27−39] These experiments typically involve electrical measurements of weakly doped single-layer graphene exposed to extremely low concentrations of NO_2. In contrast, in this study, we expose 1–10L graphene to very high NO_2 pressures in order to investigate how high hole-doping affects graphene's electronic and optical properties as a function of graphene thickness. We use micro-Raman and micro-contrast absorption spectroscopy to determine the distribution and absolute concentration of holes across the layers. These experiments help us to achieve a deeper understanding of chemical charge-transfer doping.

RESULTS AND ANALYSIS

Graphene Thickness Determination. An optical contrast spectrum is the normalized difference in reflected intensity from graphene and the quartz substrate

$$\text{contrast}(\lambda) = \frac{R_{G+Q} - R_Q}{R_Q} = \frac{4}{n_Q^2 - 1} A \qquad (1)$$

where R is reflected intensity and n_Q is the index of refraction of the substrate. The contrast is proportional

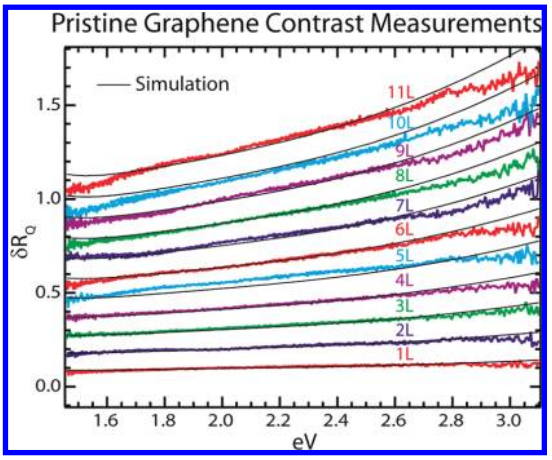

Figure 2. Contrast spectrum of 1L to 11L pristine graphene on quartz substrate. The black lines are Fresnel interference simulations.

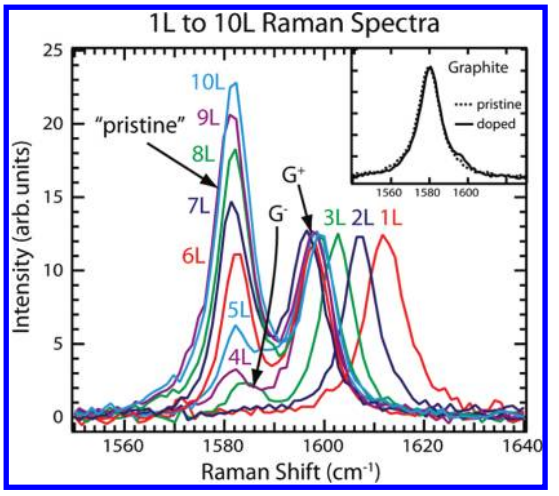

Figure 3. Raman spectra for 1L to 10L graphene on quartz exposed to 60 Torr NO_2. The spectra are normalized to the higher energy peak. The inset is the graphite spectrum before and after exposure to 60 Torr NO_2.

to graphene's absorbance, *A*. Figure 2 shows contrast data for 1−11L pristine graphene on quartz. The contrast increases with photon energy as it approaches the ultraviolet Fano peak. It also rises linearly with thickness, and we calculate an absorption at 1.45 eV (850 nm) of 2.3% per layer.

We model the contrast using Fresnel equations incorporating the phase shifts in graphene as described in the Supporting Information. The black lines in Figure 2 show the simulation results, which match the data well and provide unambiguous assignment of graphene thickness. The simulation does not match the data as well at longer and shorter wavelengths because of chromatic aberrations in the apparatus and because the graphene refractive index is not well-known beyond 750 nm.[40]

Raman Spectroscopy and Surface Chemical Doping. Raman spectra for 1−10L graphene exposed to the lower pressure (60 Torr NO_2, 30 Torr N_2O_4) are given in Figure 3. (For convenience, we often refer to NO_2 exposure, although N_2O_4 is also present above 20 Torr. Most samples were exposed to either 60 or 140 Torr NO_2.) No D peaks were present either before or after NO_2 exposure, showing that NO_2 is physisorbed, not chemisorbed, since chemisorption would create sp^3 carbons. The absolute intensity of the G peak increases with increasing thickness; here the spectra are normalized to the highest energy peak. The 1L and 2L graphene G peaks are upshifted to 1614 and 1608 cm^{-1}, respectively. The 3L graphene spectrum splits into two peaks, a higher energy peak at 1601.5 cm^{-1} and a lower energy, less intense peak at 1584 cm^{-1}. For $N \geq 4$, the peak positions remain stable at 1582 and 1598 cm^{-1}, and the intensity of the lower energy peak increases with graphene thickness. The inset shows the bulk graphite spectra, where the intensity is primarily in the lower energy peak with just a slight higher energy shoulder. This NO_2-doped Raman spectral evolution shows that NO_2 adsorbs on the top and bottom surfaces and does not intercalate, as discussed below. We fit these peaks to Voigt functions, with the Gaussian width fixed at the spectrometer resolution. The resulting Lorentzian peak fitting parameters are in Table S1, and the peak positions are plotted in Figure S1 in the Supporting Information.

The 1L graphene is heavily doped due to adsorption on both surfaces and produces a single G peak. In 2L samples, each graphene sheet is adjacent to a graphene layer and an adsorbate layer, so both sheets have the same level of doping and only a single G peak occurs (Figure 4a). This chemically induced G peak shift for 1L samples can be calibrated using electrostatically gated device graphene Raman experiments.[11,13,14] Wang and co-workers[41] found that, above a Fermi level shift of ~0.1 eV, the relationship between Fermi level shift and G peak position is linear, and we can use these results to determine our level of doping.[42] We measure a G peak position of 1618 cm^{-1} for 1L graphene after exposure to a higher pressure (140 Torr NO_2, 150 Torr N_2O_4). This G peak position corresponds to a Fermi level shift to lower energy of 0.86,[11] 0.83,[14] 0.68,[41] or 0.55 eV,[13] depending upon the reference. The absence of the Raman 2D peak, as discussed below, indicates that higher values at 0.86 and 0.83 eV are correct. We can convert the 0.83 eV Fermi level shift to a hole density using the equation $E_F = -\hbar v_F(\pi|n|)^{1/2}$ ($v_F = 1.1 \times 10^6$ m/s).[1,43] This yields a hole density of 4.5×10^{13} cm^{-2}, about one hole for every 100 graphene carbon atoms.

For both electrostatically doped graphene in gated devices[13,14,44] and chemically charge-transfer-doped graphene,[5,6,19,21] the 2D peak intensity decreases as the doping level increases. In a similar fashion, we observe that the 2D/G ratio deceases with doping level in Figure 5. In this figure, the initial pristine graphene ratio can vary by a factor of 2 due to sample inhomogeneity.[45] This 2D/G ratio in the presence of NO_2 gives us an independent check on the Fermi level

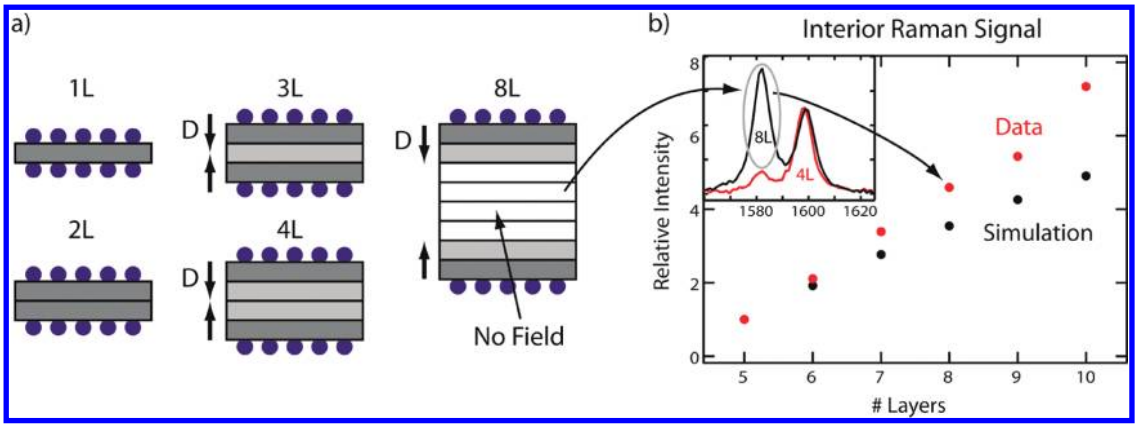

Figure 4. (a) Schematic of graphene doping by NO_2 surface adsorption. Dark gray, light gray, and white layers are heavily doped, lightly doped, and not doped, respectively. The arrows indicate the resultant electric fields. (b) Normalized data and Fresnel interference simulation of the relative intensity of the G peak of undoped interior layers for $N > 4$. The inset shows how, for the 8L spectrum, subtracting the 4L spectrum can generate the normalized G peak signal for the innermost pristine layers. The graphene is on a quartz substrate and exposed to 60 Torr NO_2.

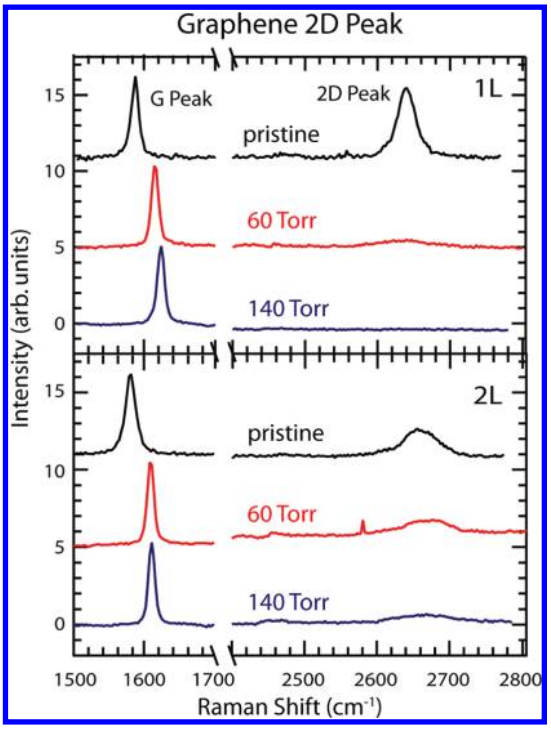

Figure 5. G peak and 2D peak Raman spectrum for monolayer and bilayer graphene on quartz. The spectra are for pristine, 60 Torr NO_2 exposed, and 140 Torr NO_2 exposed graphene.

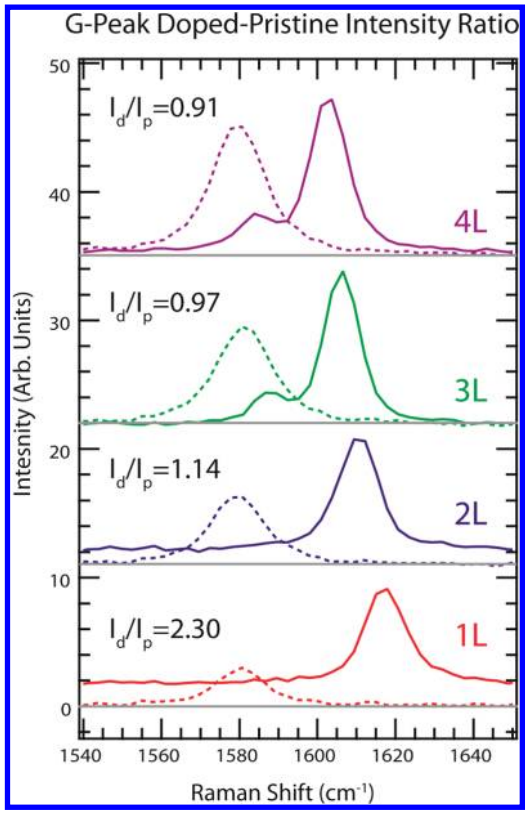

Figure 6. Raman spectra of 1L to 4L graphene G peak exposed to 140 Torr NO_2 on 290 nm SiO_2/Si substrate. The dashed and solid lines are pristine and NO_2-exposed graphene, respectively. The gray lines are the baseline for each graphene thickness. I_d/I_p is the doped/pristine graphene G peak intensity ratio. The 1L and 2L NO_2-doped graphene have a background signal. All spectra are normalized to the silicon peak at ~950 cm^{-1}.

shift. The 2D band strong resonance Raman effect is lost when the laser excitation energy E_{ex} minus the 2D energy is less than twice the Fermi level shift E_F: $E_{ex} - \hbar\omega_{2D} < 2E_F$.[6,41] Thus, since we do not detect the associated 2D peak, we conclude that $E_F \geq 0.82$ eV for our 1L graphene at 140 Torr NO_2. For 2L graphene, the 2D peak also decays but does not disappear at 140 Torr, consistent with the lower level of doping expected for surface adsorption of 2L samples compared to 1L.

We observe that the G peak changes in absolute intensity as well as position when the graphene is this highly doped. Figure 6 shows the intensity of 1L to 4L graphene on a 290 nm SiO_2/Si substrate. Spectra are normalized to the substrate silicon overtone peak at ~950 cm^{-1}. The intensity ratio for the doped G peak to the pristine G peak is 2.3 for 1L graphene,

1.14 for 2L graphene, and essentially 1 for thicker samples and cannot be explained by additional reflections and interference involving the adsorbed molecular layers.[46]

A resonant increase in the absolute G peak Raman intensity was first observed in heavily hole-doped graphite intercalation compounds[47] and recently was also observed in electrochemically doped monolayer graphene and bilayer graphene heavily electron doped by adsorbed alkalis.[3,48] Graphene with single gate electrostatic hole-doping shows resonant increase in G peak intensity, reaching a maximum at $2E_F = E_{ex} - \hbar\omega_G/2$.[41,49] Following the theory of Basko,[50] this behavior represents a change in Raman pathway quantum interference as doping increases. Transitions that originate above and below the resonant transition $E_{ex} - \hbar\omega_G/2$ have opposite phase and interfere destructively. As a result, less destructive interference and a larger Raman G peak intensity occur for Fermi level shifts up to $E_{ex} - \hbar\omega_G/2$, at which point the signal begins decreasing. This trend indicates the importance of nonresonant transitions in the G peak intensity. For 140 Torr NO_2, $2E_F$ = 1.66 eV for 1L graphene, which is approaching the expected resonance maximum at $E_{ex} - \hbar\omega_G/2$ = 1/86 eV. For $N > 2$, the Fermi level shift does not approach the excitation energy closely enough to generate this intensity enhancement. This result shows that we observe the quantum interference effect for chemically doped graphene, confirming the importance of nonresonant scattering pathways. G mode intensity increase is an additional and independent measurement of Fermi level shift.

Figure 6 also shows that a scattering continuum develops for 1L and 2L, after exposure to NO_2, along with the absolute G band intensity increase. This continuum is not present in undoped graphene or thicker doped samples. This could be "hot" graphene luminescence, as was observed to occur simultaneously with the G mode resonance for one-sided electrostatic device gating.[41]

For $N > 2$ graphenes, charge-transfer doping is more complex: we observe two Raman G modes. Bilayer graphene is known to show two G peaks in the presence of a perpendicular electric field,[51−54] which can be created, for example, by top and bottom gates of opposite bias in field-effect devices.[51,52,54] In bilayer graphene, the G modes of each layer are coupled, forming a symmetric, in-phase Raman-active mode and an antisymmetric, out-of-phase Raman-inactive mode.[51,52,54] The electric field reduces the graphene bilayer symmetry by removing the inversion center, and the new eigenstates G^+ and G^- are linear combinations of the in-phase and out-of-phase modes. The intensity of each peak comes from the in-phase Raman G mode contribution. A strong perpendicular electric field can open up a band gap of ~0.3 eV in 2L graphene.[51,55]

Our 2L sample has a single G peak, which indicates symmetric doping from adsorption on both sides, and there is no net electric field between the layers. In our $N > 2$ samples, the G peak splitting shows that doping is primarily in the surface graphene layers, creating perpendicular electric fields that point inward. The interior layers have lower hole density. This situation could also be created by use of top and bottom gates of the same voltage in a device configuration. These fields polarize the interior layers, creating partial screening of the fields. When the Raman peaks stop shifting position with N, the electric field no longer penetrates into the graphene center. Thus, we conclude from our data that for $N > 4$ the outermost 2L on each surface contains non-negligible doping while interior layers are undoped and experience no electric field, as shown in Figure 4a.

As our samples become thicker, more electronic bands are present, the doping varies with layer, and G modes mix to form normal modes extending over the doped sample. While a rigorous theory is not available, a simple local model provides insight into the G peak evolution. We postulate 2L-thick doped surface regions with an intrinsic interior region. For $N \geq 5$, the outer 2L on each graphene surface produces a 4L-like peak, and the interior layers are pristine. We normalize 4L and thicker samples to the G^+ integrated peak intensity and subtract the G^- 4L peak from the pristine/G^- peak of thicker samples, as shown in the Figure 4b inset for 8L. The difference is normalized to the 5L subtracted value. We perform a Fresnel interference simulation of the expected Raman signal from these interior layers using the equations from Yoon *et al.*,[56] integrating over the interior layers. Including the adsorbed molecular layer in the calculation changes the result by less than 1%. The refractive indices are given in the Supporting Information. The data and simulation agree well for thinner graphenes but deviate by up to 30% for thicker samples. Previous ARPES measurements with similar doping density to our experiments found that for 3- and 4-layer graphene, the majority of the charge is in the first layer, with less than 10 and 15% in the second layer, respectively.[57] Given a constant carrier concentration with thickness for our samples, this increase in charge penetration in thicker graphene would lead to a weaker electric field and an increase in I_{G-} relative to I_{G+}.[51,52,57] This trend would bring the data in Figure 4b more in line with the calculation. These results are also consistent with theory, which shows that charge concentrations on the order of 10^{13} cm^{-2} should give typical screening depths of two to three monolayers.[55,58] This simple model confirms that few-layer graphene samples efficiently screen perpendicular electric fields created by surface charge transfer.

We can use the established bilayer Raman theory to help understand the relative G mode Raman intensities and band gap openings near the surface in our larger

N samples. Most of the doped charge is in the top and bottom layers. Recall that 1L graphene alone shows a doped charge density of 3.6×10^{13} cm^{-2} for 60 Torr NO_2. We might assume that the total charge density for $N > 1$ is also about 3.6×10^{13} holes/cm^2, with 1.8×10^{13} holes/cm^2 present on the top and bottom layers for thicker samples. Ando and Koshino modeled the band gap, the G^+ and G^- peak positions, and the G^+ and G^- relative intensities for electrically gated bilayer graphene. Their results for one-sided gating are most relevant to understand individual surfaces of our thicker samples. If we use a surface charge concentration of 1.8×10^{13} holes/cm^2, then Ando and Koshino predict an I_{G-}/I_{G+} intensity ratio of ~0.25, slightly higher than our 4L value of 0.18. For this charge concentration, they predict a band gap of 0.15 eV in the 2L-like bands in the surface region. They also calculate a downshift of the G^- peak position at these charge densities but exclude electron–hole asymmetry. Mauri and co-workers include these effects, and they predict G^- and G^+ peak positions of 1582 and 1591 cm^{-1}, with a relative intensity of 0.30 in reasonable agreement with our data.[52] For both of these calculations, the intensity ratio reaches an asymptote of about 0.25 for doping above 2.5×10^{13} holes/cm^2. This band gap is much larger than the 30 meV band gap observed in low-temperature ARPES measurements of epitaxially grown bilayer graphene doped on one side by a low pressure of NO_2.[59]

We make a direct comparison between the 1L and 4L results and previous surface doping by iodine;[5] 0.1 Torr I_2 adsorbs on the top and bottom graphene surfaces, and electron transfer forms I_3^- and I_5^-. For 1L, NO_2 and I_2 generate 3.6 and 2.6×10^{13} holes/cm^2, respectively, while the NO_2 pressure is 600 times larger than that of iodine. The electron affinities for NO_2 and I_2 are similar (2.3 and 2.5 eV). The unexpectedly low doping despite a larger pressure is due to differences in surface coverage of the species involved. At higher pressures, NO_2 exists on the surface primarily as N_2O_4.[60,61] Conversely, I_2 adsorbs and forms I_3^- and I_5^- after charge transfer, so its coverage is not limited. For 3L and 4L, the NO_2 G peaks are in the same position as I_2-doped graphene, and the intensity ratios are similar, indicating similar doping depth and electric field strength. For these experiments, and for doping by sulfuric acid,[18] the 1L G peak is noticeably wider than other peaks, the opposite of expectations. We attribute this widening to sample inhomogeneity.

NO_2 Langmuir Adsorption Isotherm. In Figure 5, the G peak upshifts more at higher NO_2 pressures, showing that chemical charge-transfer doping can be adjusted by changing the dopant surface density. The adsorbed NO_2 concentration should be related to the NO_2 pressure *via* a Langmuir adsorption isotherm. By determining the graphene hole concentration in 1L graphene from the G-peak upshift, we might relate θ, the fractional charge transferred to graphene per C atom, to the pressure *P via* a modified Langmuir isotherm (eq 2).

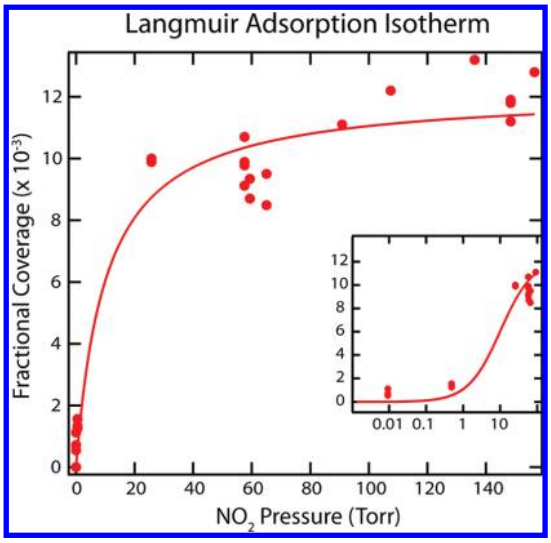

Figure 7. Modified Langmuir adsorption isotherm as a function of NO_2 pressure. The inset is the same data and fit on a log scale so low pressure points can be seen more easily.

$$\theta(P) = \theta_{max} \frac{KP}{1 + KP} \quad (2)$$

K is the equilibrium constant between the gas and the surface. We convert the G peak shift to a hole density using the previously described device gating Raman experiments. We divide this value by the graphene carbon atom density to get a fractional charge transfer. Figure 7 shows the fractional charge transfer as a function of NO_2 pressure for 1L graphene. This model is complicated by the equilibrium between NO_2 and N_2O_4. Below 20 Torr pressure, NO_2 is dominant in the gas phase; electrical NO_2 doping experiments and theory find that for low adsorption densities one electron is transferred for each NO_2 molecule.[25,26] At higher pressures, experiments on graphite and grafoil indicated that NO_2 adsorbs primarily as N_2O_4.[60,61] Thus, both adsorbed N_2O_4 and NO_2 may contribute to doping if electron transfer to each N_2O_4 is a small fraction of an electron.

In Figure 7, the data fit the isotherm yielding $\theta_{max} = 0.012$ and $K = 0.10$ Torr^{-1}. The charge transfer clearly reaches a plateau at higher pressures, indicating monolayer coverage, and θ_{max} corresponds to 1.2% of carbon atoms transfer an electron to the adsorbed monolayer. Reevacuating a sample exposed to 60 Torr NO_2 (30 Torr N_2O_4) does not regenerate pristine graphene. Significant doping remains as shown by the G mode at 1605 cm^{-1} for 1L graphene (not shown). This corresponds to a hole density of 2×10^{13} cm^{-1}, compared to the exposed density of 3.6×10^{13} cm^{-1}. This result reflects a significant binding energy for

some unknown (perhaps anionic) nitrogen oxide species to graphene. The binding energy of NO_2 on graphite has been measured by thermal desorption spectra as 0.4 eV[61,62] and calculated at 0.06 eV,[63] although the low-temperature desorption measurement may actually reflect more N_2O_4 than NO_2. For $N \geq 2$, there is little pressure dependence of the spectra above 40 Torr of NO_2, which indicates stronger adsorption on thicker graphenes. The 1L graphene on SiO_2 has ridges and ripples absent from thicker samples.[64] This morphology adds weak sp^3 character to the graphene sheets and decreases the π bonding network that is crucial to adsorption.

Optical Contrast Measurement of Chemical Charge-Transfer Doping. Thus far, we have determined the charge-transfer graphene hole density from the Raman data using the self-consistency of the G peak position and absolute intensity and the 2D/G intensity ratio; in addition, we also observe the effect of the high degree of charge transfer in the graphene optical absorption spectrum. Graphene doping creates an π to π^* interband optical absorption threshold at a photon energy of $2E_F$,[41,65,66] as originally observed in highly doped graphite intercalation compounds decades ago.[47] Figure 8a compares optical contrast before and after exposure to 140 Torr NO_2 (recall that contrast is proportional to absorbance). The optical contrast in doped 1L graphene drops to zero near 1.5 eV; contrast in 2L drops by about half near 1.5 eV, and thicker samples drop progressively smaller fractions until 10L and 11L both show essentially no change. The additional reflections and interference effects of NO_2/N_2O_4 adsorbed layers have a negligible optical effect on the contrast measurements, as is discussed in more detail in the Supporting Information. We subtract the pristine spectrum from the doped spectrum to obtain the NO_2-induced change in contrast (Figure 8b for 1L).

We fit these spectra to a step function absorption spectrum with Lorentzian broadening to represent fast excited state decay. The amplitude of the NO_2-induced contrast difference is fixed at an absorbance of 2.3% per layer (or $\delta R_Q = 0.0812$ per layer for $n_s = 1.46$) because for thicker samples the contrast spectrum never fully decays. The fit results are given in Table S2 in the Supporting Information. The graphene absorption cutoff goes to lower energy as the graphene sample becomes thicker. Since the NO_2 adsorption is on both the top and the bottom surfaces of graphene, regardless of thickness, the charge transfer should be the same in each case. The absorption cutoff shifts to lower energy with increasing graphene thickness because thicker graphenes have more electronic bands, and the density of states is expected to increase more rapidly with energy, thus slowing the state filling. The lifetime broadening is ~0.2 eV (fwhm). The 1L and 2L fits are robust, but thicker graphene fits will be less reliable

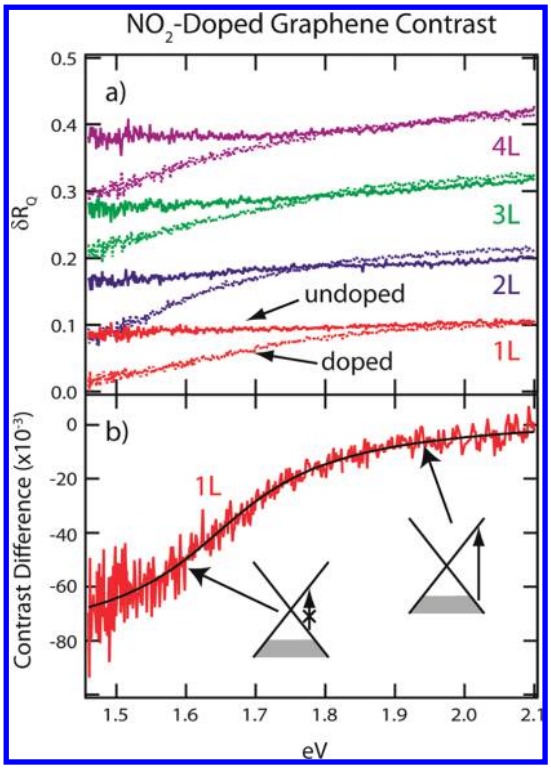

Figure 8. (a) Contrast data for 1L to 4L graphene on quartz. The solid lines are pristine graphene, and the dotted lines are graphene exposed to 140 Torr NO_2. (b) NO_2-induced change in contrast for 1L graphene. This is the pristine spectrum subtracted from the doped spectrum in (a). The black line is the fit.

because the absorption has decayed <30% in our energy range.

For 1L graphene, we make a direct comparison of the Fermi level shift from Raman and contrast data. The optical absorption cutoff occurs at 1.65 eV, giving a decrease in the Fermi level of 0.83 eV, in agreement with the shift determined above from Raman spectroscopy. This direct measurement of the Fermi level, in combination with the Raman G peak, shows that calibrating the chemical doping using gated field device experiments is reliable. This relationship between G peak and doping level is also in good agreement with the Raman and absorption studies performed by Wang and co-workers, who simultaneously measured the G peak shift and interband absorption cutoff in single gate devices.[41] Wang and co-workers also measured an excited state lifetime of 0.4 eV, in reasonable agreement with our 0.2 eV value.

The Fermi level shift for 2L graphene exposed to 140 Torr NO_2 is 0.77 eV, only slightly lower than that of 1L. Such a small drop from 1L to 2L is unexpected, given that 2L graphene should accept roughly twice as many electrons for the same Fermi level shift as 1L graphene. Raman spectra of I_3^- and I_5^- anions on graphene previously showed less charge transfer on 1L than on 2L graphene.[67] A similar effect was found for Li^+ adsorbed on few layer graphene.[68] In each case, the

lower than expected charge transfer on 1L graphene was attributed to ion repulsion between the top and bottom molecular adsorbents. We attribute our lower than expected 1L doping to this effect.

Chemically Charge-Transfer-Doped Graphenes as Electronic Materials. We have seen in this work that an essentially quantitative understanding of few-layer thick graphenes doped by charge transfer from adsorbed species can be achieved by purely optical characterization: Raman and contrast absorption measurements. We also see that chemical charge-transfer doping produces essentially the same optical response as gated electrostatic doping in devices: both methods produce delocalized mobile electrical carriers in the graphene planes.

The intrinsic 2D nature of graphene makes charge-transfer doping promising for creating a class of graphene electronic materials with a wide range of properties. Highly doped graphene is very different than intrinsic graphene. Before exposure to NO_2, our pristine graphene samples actually have a very low doping of about 1 carrier per 10^4 C atoms due to interactions with the substrate and the atmosphere; in our NO_2-exposed graphene, the carrier density is 2 orders of magnitude higher. Highly doped graphene is an almost perfectly transparent, highly conductive 2D metallic membrane. As we have seen, an E_F of 1 eV produces an absorption threshold of 2 eV in the visible spectrum. With NO_2 doping, we achieve substantial transparency in the near-IR; highly electron-doped few-layer graphenes show substantial transparency in the visible.[3]

Few-layer graphenes are doped strictly by surface adsorption both in our present NO_2 studies and in earlier I_2 studies.[5,67] In Br_2,[67] alkali atom,[3] and $FeCl_3$[6] studies, doping occurs by intercalation between layers as well as by adsorption. Intercalated molecules were observed to transfer more charge than surface-adsorbed layers of the same species.[3,6,67] This likely results from both the lower local dielectric constant of the surface environment, resulting in greater ion repulsion as discussed above, and enhanced local chemical bonding in the intercalated materials. In addition, the extent (or staging behavior) of intercalation can be varied and controlled by the molecular species chemical potential (typically pressure or concentration). A wide variety of situations can be created. Also note that charge-transfer doping can be more versatile than traditional substitutional doping of N or B atoms for C in the graphene plane. In 3D semiconductors such as silicon, substitutional dopants quantitatively produce free carriers at room temperature, as the Coulomb interaction between carrier and ionized dopant is strongly screened. In 2D graphene with every atom on the surface, screening is reduced.[69] The Coulomb interaction is stronger, and the introduced carrier is only partially released as observed in a recent study of N substitution.[70]

With charge-transfer doping, high carrier densities can be easily achieved, as shown optically in the present NO_2 work and shown electrically in a recent study of hole-doped, Br_2-intercalated graphite.[71,72] In this Br_2 study, very high carrier mobility was observed at high hole density. Carrier mobility was not substantially reduced by scattering from charged dopants in the Br_2 layers. In substitutional doping, scattering from charged dopants in the same graphene plane as the carriers would be significant. The advantage of few-layer graphene charge-transfer doping, in separating carriers from charged acceptors, is similar to that of modulation doping in 2D GaAs/AlGaAs and silicon–germanium semiconductor superlattices.[73−75] It will be important to directly measure mobilities in few-layer graphenes doped by chemical charge transfer.

When we expose bilayer graphene to NO_2, the graphene is doped equally from both sides, as judged from the observation of only a single Raman G mode. The sample is supported on SiO_2, which is not atomically smooth. Graphene is not hermetically sealed to the SiO_2, and gas penetrates underneath. On an atomically flat substrate such as hexagonal BN, bilayer graphene should be more effectively sealed. Hexagonal BN is a large band gap insulator, and it should not dope graphene. In this situation, exposure to NO_2 should dope graphene on only one side, similar to one-sided electrostatic gating. In this situation, a bilayer will develop a band gap, in addition to undergoing a Fermi level shift. If one could find some way to dope the bilayer equally and oppositely on both sides, a band gap would open without a Fermi level shift. This might be done by use of electronegative and electropositive polymers on opposite sides.

CONCLUSIONS

These experiments demonstrate that detailed, quantitative information on high hole-doped graphene can be determined directly from spectroscopic measurements. The graphene Raman G peak for 1L to 10L graphene shows that NO_2 adsorbs equally on both sides, and that the delocalized holes exist primarily in the two layers closest to the surface. Contrast spectroscopy directly measured a Fermi level shift of 0.83 eV and a corresponding carrier density of 4.5×10^{13} holes/cm^2. The G peak position, intensity, and 2D peak intensity can also give the Fermi level shift and are consistent with this result. For 1L graphene, an increased G peak intensity upon adsorption indicates the presence of quantum interference and the importance of nonresonant pathways for the Raman signal. We were able to control the Fermi level and hole concentration by varying the molecular surface density.

Pressure-dependent measurements of the G peak position show that for high pressures the doping saturates, indicating the presence of a molecular monolayer composed of NO_2 and N_2O_4.

METHODS

We generate graphene flakes by mechanical exfoliation of Kish graphite (Covalent Materials, Size B) in air. These flakes were primarily deposited onto piranha-cleaned quartz slides, although several experiments were done on 290 nm SiO_2/Si substrates. We verify graphene thickness by contrast spectroscopy and place the sample into a quartz cuvette cell, which is connected to a vacuum system and a liquid NO_2 cylinder (Matheson Tri-Gas Chemically Pure, 99.5%) supplying 1 atm of NO_2. A diffusion pump evacuates the system to 1×10^{-4} Torr, and a fixed volume of NO_2 gas expands into the sample cell. This procedure produces typical NO_2 pressures of 60 Torr, although the NO_2 pressure can be adjusted within a limited set of values by changing the initial gas volume and the subsequent expansion volume. We determine the pressure from UV−vis absorption. Gaseous NO_2 exists in equilibrium with N_2O_4, which is diamagnetic and weakly doping.[39] A typical NO_2−N_2O_4 spectrum is given in Figure S2 in the Supporting Information. The 340 nm N_2O_4 peak is narrow, while the 400 nm NO_2 peak is broader and contains vibrational structure. For convenience, we refer to NO_2 exposure, although N_2O_4 is also present above 20 Torr. We fit these peaks to Gaussians and use the peak absorbances, along with absorption cross sections of 6.18×10^{-21} cm^2/molecule and 6.65×10^{-21} cm^2/molecule to obtain the number density for NO_2 and N_2O_4, respectively.[76] Over our pressure range, both the ideal gas law and the van der Waals equation generate the same pressure from this number density. Most of the samples were exposed to a lower pressure (60 Torr NO_2, 30 Torr N_2O_4) or a higher pressure (140 Torr NO_2, 150 Torr N_2O_4).

For contrast measurements, a quartz−tungsten halogen lamp (Oriel) sends light through a 100 μm pinhole, which is collimated by an $f = 300$ mm lens doublet. An iris cuts the beam diameter to 2 mm to minimize chromatic aberrations. The light enters an inverted microscope where a 40×/0.6 NA objective focuses it to a 2 μm diameter. The reflected spectrum enters a 0.27 m monochromator and strikes a CCD array detector with 1 nm resolution. For longer wavelengths, we use a 650 nm long pass filter to eliminate second order diffractions of shorter wavelength light. We calibrate the spectrum using a holmium perchlorate solution (Sigma Aldrich H8015-3mL). Micro-Raman measurements are taken using the same experimental setup. We use 4 mW of 632.8 nm helium−neon laser light focused to a 1 μm spot diameter, averaged for 15 min with 3.5 or 7 cm^{-1} resolution, depending on the spectrometer grating. The use of 632.8 nm light avoids NO_2 absorption and fluorescence (Figure S2).

Conflict of Interest: The authors declare no competing financial interest.

Acknowledgment. This work on chemical charge transfer to graphene has been supported by the DOE Solar Energy Program under DE-FG02-11ER16224. We have enjoyed stimulating discussions with P. Kim, T. Heinz, J. Hone, M. Steigerwald, E. Thrall, Z. Chen, Y. Guo, and Z. Yu. We thank K.F. Mak for advice on the contrast measurements, and Steffen Jockusch for experimental advice and access to the vacuum apparatus. We thank A. Grigorenko for sharing graphene refractive index data, and D.M. Basco of CNRS for enlightening correspondence on graphene Raman theory.

Supporting Information Available: UV−visible absorption spectrum of gas-phase NO_2 and N_2O_4. Details on the pristine graphene contrast spectrum simulations, a discussion of how the adsorbed molecular layers affect the contrast measurements, the fit parameters for Raman and contrast data, and complete references for 14, 41, 65, and 70. This material is available free of charge *via* the Internet at http://pubs.acs.org.

REFERENCES AND NOTES

1. Zhang, Y. B.; Tan, Y. W.; Stormer, H. L.; Kim, P. Experimental Observation of the Quantum Hall Effect and Berry's Phase in Graphene. *Nature* **2005**, *438*, 201–204.
2. Guerard, D.; Foley, G. M. T.; Zanini, M.; Fischer, J. E. Electronic-Structure of Donor-Type Graphite Intercalation Compounds. *Nuovo Cimento Soc. Ital. Fis., B* **1977**, *38*, 410–417.
3. Jung, N.; Kim, B.; Crowther, A. C.; Kim, N.; Nuckolls, C.; Brus, L. Optical Reflectivity and Raman Scattering in Few-Layer-Thick Graphene Highly Doped by K and Rb. *ACS Nano* **2011**, *5*, 5708–5716.
4. Yang, M. H.; Eklund, P. C. Optical Dielectric Function of High-Stage Potassium Graphite-Intercalation Compounds-Experiment and Theory. *Phys. Rev. B* **1988**, *38*, 3505–3516.
5. Jung, N.; Kim, N.; Jockusch, S.; Turro, N. J.; Kim, P.; Brus, L. Charge Transfer Chemical Doping of Few Layer Graphenes: Charge Distribution and Band Gap Formation. *Nano Lett.* **2009**, *9*, 4133–4137.
6. Tan, P. H.; Zhao, W. J.; Liu, J.; Ferrari, A. C. Intercalation of Few-Layer Graphite Flakes with $FeCl_3$: Raman Determination of Fermi Level, Layer by Layer Decoupling, and Stability. *J. Am. Chem. Soc.* **2011**, *133*, 5941–5946.
7. Dresselhaus, M. S.; Dresselhaus, G. Intercalation Compounds of Graphite. *Adv. Phys.* **2002**, *51*, 1–186.
8. Underhill, C.; Leung, S. Y.; Dresselhaus, G.; Dresselhaus, M. S. Infrared and Raman-Spectroscopy of Graphite-Ferric Chloride. *Solid State Commun.* **1979**, *29*, 769–774.
9. Partoens, B.; Peeters, F. M. From Graphene to Graphite: Electronic Structure around the K Point. *Phys. Rev. B* **2006**, *74*, 075404.
10. Pisana, S.; Lazzeri, M.; Casiraghi, C.; Novoselov, K. S.; Geim, A. K.; Ferrari, A. C.; Mauri, F. Breakdown of the Adiabatic Born-Oppenheimer Approximation in Graphene. *Nat. Mater.* **2007**, *6*, 198–201.
11. Yan, J.; Zhang, Y. B.; Kim, P.; Pinczuk, A. Electric Field Effect Tuning of Electron−Phonon Coupling in Graphene. *Phys. Rev. Lett.* **2007**, *98*, 166802.
12. Ando, T. Anomaly of Optical Phonon in Monolayer Graphene. *J. Phys. Soc. Jpn.* **2006**, 75.
13. Das, A.; Chakraborty, B.; Piscanec, S.; Pisana, S.; Sood, A. K.; Ferrari, A. C. Phonon Renormalization in Doped Bilayer Graphene. *Phys. Rev. B* **2009**, *79*, 155417.
14. Das, A.; Pisana, S.; Chakraborty, B.; Piscanec, S.; Saha, S. K.; Waghmare, U. V.; Novoselov, K. S.; Krishnamurthy, H. R.; Geim, A. K.; Ferrari, A. C.; *et al.* Monitoring Dopants by Raman Scattering in an Electrochemically Top-Gated Graphene Transistor. *Nat. Nanotechnol.* **2008**, *3*, 210–215.
15. Basko, D. M.; Piscanec, S.; Ferrari, A. C. Electron−Electron Interactions and Doping Dependence of the Two-Phonon Raman Intensity in Graphene. *Phys. Rev. B* **2009**, *80*, 165413.
16. Eklund, P. C.; Smith, D. S.; Murthy, V. R. K.; Leung, S. Y. Optical Studies of the High-Frequency Graphitic Intralayer Phonons in Graphite-$SbCl_5$. *Synth. Met.* **1980**, *2*, 99–107.
17. Gualberto, G. M.; Underhill, C.; Leung, S. Y.; Dresselhaus, G. Raman and Infrared-Spectra of Graphite-$AlCl_3$. *Phys. Rev. B* **1980**, *21*, 862–868.
18. Zhao, W. J.; Tan, P. H.; Zhang, J.; Liu, J. A. Charge Transfer and Optical Phonon Mixing in Few-Layer Graphene Chemically Doped with Sulfuric Acid. *Phys. Rev. B* **2010**, *82*, 245423.
19. Das, B.; Voggu, R.; Rout, C. S.; Rao, C. N. R. Changes in the Electronic Structure and Properties of Graphene Induced by Molecular Charge-Transfer. *Chem. Commun.* **2008**, 5155–5157.
20. Rao, C. N. R.; Voggu, R. Charge-Transfer with Graphene and Nanotubes. *Mater. Today* **2010**, *13*, 34–40.

21. Voggu, R.; Das, B.; Rout, C. S.; Rao, C. N. R. Effects of Charge Transfer Interaction of Graphene with Electron Donor and Acceptor Molecules Examined Using Raman Spectroscopy and Cognate Techniques. *J. Phys.: Condens. Matter* **2008**, *20*, 472204.
22. Mak, K. F.; Sfeir, M. Y.; Wu, Y.; Lui, C. H.; Misewich, J. A.; Heinz, T. F. Measurement of the Optical Conductivity of Graphene. *Phys. Rev. Lett.* **2008**, *101*, 196405.
23. Nair, R. R.; Blake, P.; Grigorenko, A. N.; Novoselov, K. S.; Booth, T. J.; Stauber, T.; Peres, N. M. R.; Geim, A. K. Fine Structure Constant Defines Visual Transparency of Graphene. *Science* **2008**, *320*, 1308–1308.
24. Mak, K. F.; Shan, J.; Heinz, T. F. Seeing Many-Body Effects in Single- and Few-Layer Graphene: Observation of Two-Dimensional Saddle-Point Excitons. *Phys. Rev. Lett.* **2011**, *106*, 046401.
25. Schedin, F.; Geim, A. K.; Morozov, S. V.; Hill, E. W.; Blake, P.; Katsnelson, M. I.; Novoselov, K. S. Detection of Individual Gas Molecules Adsorbed on Graphene. *Nat. Mater.* **2007**, *6*, 652–655.
26. Leenaerts, O.; Partoens, B.; Peeters, F. M. Paramagnetic Adsorbates on Graphene: A Charge Transfer Analysis. *Appl. Phys. Lett.* **2008**, *92*, 243125.
27. Dua, V.; Surwade, S. P.; Ammu, S.; Agnihotra, S. R.; Jain, S.; Roberts, K. E.; Park, S.; Ruoff, R. S.; Manohar, S. K. All-Organic Vapor Sensor Using Inkjet-Printed Reduced Graphene Oxide. *Angew. Chem., Int. Ed.* **2010**, *49*, 2154–2157.
28. Ghosh, A.; Late, D. J.; Panchakarla, L. S.; Govindaraj, A.; Rao, C. N. R. NO_2 and Humidity Sensing Characteristics of Few-Layer Graphene. *J. Exp. Nanosci.* **2009**, *4*, 313–322.
29. Han, T. H.; Huang, Y. K.; Tan, A. T. L.; Dravid, V. P.; Huang, J. X. Steam Etched Porous Graphene Oxide Network for Chemical Sensing. *J. Am. Chem. Soc.* **2011**, *133*, 15264–15267.
30. Jeong, H. Y.; Lee, D. S.; Choi, H. K.; Lee, D. H.; Kim, J. E.; Lee, J. Y.; Lee, W. J.; Kim, S. O.; Choi, S. Y. Flexible Room-Temperature NO_2 Gas Sensors Based on Carbon Nanotubes/Reduced Graphene Hybrid Films. *Appl. Phys. Lett.* **2010**, *96*, 213105.
31. Ko, G.; Kim, H. Y.; Ahn, J.; Park, Y. M.; Lee, K. Y.; Kim, J. Graphene-Based Nitrogen Dioxide Gas Sensors. *Curr. Appl. Phys.* **2010**, *10*, 1002–1004.
32. Lu, G. H.; Ocola, L. E.; Chen, J. H. Gas Detection Using Low-Temperature Reduced Graphene Oxide Sheets. *Appl. Phys. Lett.* **2009**, *94*, 083111.
33. Lu, G. H.; Ocola, L. E.; Chen, J. H. Reduced Graphene Oxide for Room-Temperature Gas Sensors. *Nanotechnology* **2009**, 20.
34. Lu, G. H.; Park, S.; Yu, K. H.; Ruoff, R. S.; Ocola, L. E.; Rosenmann, D.; Chen, J. H. Toward Practical Gas Sensing with Highly Reduced Graphene Oxide: A New Signal Processing Method To Circumvent Run-to-Run and Device-to-Device Variations. *ACS Nano* **2011**, *5*, 1154–1164.
35. Nomani, M. W. K.; Shishir, R.; Qazi, M.; Diwan, D.; Shields, V. B.; Spencer, M. G.; Tompa, G. S.; Sbrockey, N. M.; Koley, G. Highly Sensitive and Selective Detection of NO_2 Using Epitaxial Graphene on 6h-SiC. *Sens. Actuators, B* **2010**, *150*, 301–307.
36. Pearce, R.; Iakimov, T.; Andersson, M.; Hultman, L.; Spetz, A. L.; Yakimova, R. Epitaxially Grown Graphene Based Gas Sensors for Ultra Sensitive NO_2 Detection. *Sens. Actuators, B* **1022**, *155*, 451–455.
37. Qazi, M.; Nomani, M. W. K.; Chandrashekhar, M. V. S.; Shields, V. B.; Spencer, M. G.; Koley, G. Molecular Adsorption Behavior of Epitaxial Graphene Grown on 6h-SiC Faces. *Appl. Phys. Express* **2010**, *3*, 075101.
38. Song, X.; Wagner, B.; Kang, Z. A Chemical Gas Sensor from Large-Scale Thermal CVD Derived Graphene. *Mater. Res. Soc. Symp. Proc.* **2011**, *1303*, 151–156.
39. Wehling, T. O.; Novoselov, K. S.; Morozov, S. V.; Vdovin, E. E.; Katsnelson, M. I.; Geim, A. K.; Lichtenstein, A. I. Molecular Doping of Graphene. *Nano Lett.* **2008**, *8*, 173–177.
40. Kravets, V. G.; Grigorenko, A. N.; Nair, R. R.; Blake, P.; Anissimova, S.; Novoselov, K. S.; Geim, A. K. Spectroscopic Ellipsometry of Graphene and an Exciton-Shifted Van Hove Peak in Absorption. *Phys. Rev. B* **2010**, *81*, 155413.
41. Chen, C. F.; Park, C. H.; Boudouris, B. W.; Horng, J.; Geng, B. S.; Girit, C.; Zettl, A.; Crommie, M. F.; Segalman, R. A.; Louie, S. G.; *et al.* Controlling Inelastic Light Scattering Quantum Pathways in Graphene. *Nature* **2011**, *471*, 617–620.
42. The samples in these experiments were in some cases intrinsically doped up to 1590 cm^{-1}, but for the very high doping conditions of our NO_2 adsorption experiments, pristine graphene with intrinsic doping at 1581 and 1590 cm^{-1} yielded the same final G peak shift upon exposure to 60 Torr NO_2. This is likely due to the higher density of states at large Fermi level shifts, where intrinsic doping concentrations have a small effect.
43. Novoselov, K. S.; Geim, A. K.; Morozov, S. V.; Jiang, D.; Katsnelson, M. I.; Grigorieva, I. V.; Dubonos, S. V.; Firsov, A. A. Two-Dimensional Gas of Massless Dirac Fermions in Graphene. *Nature* **2005**, *438*, 197–200.
44. Casiraghi, C. Doping Dependence of the Raman Peaks Intensity of Graphene Close to the Dirac Point. *Phys. Rev. B* **2009**, *80*, 233407.
45. Casiraghi, C.; Pisana, S.; Novoselov, K. S.; Geim, A. K.; Ferrari, A. C. Raman Fingerprint of Charged Impurities in Graphene. *Appl. Phys. Lett.* **2007**, *91*, 233108.
46. We performed Fresnel interference simulations which showed that the molecular layers would actually decrease the Raman intensity for $N = 1-4$ by about 30%. Thus, the intensity increase is caused by the quantum interference effect.
47. Eklund, P. C.; Mahan, G. D.; Spolar, J. G.; Arakawa, E. T.; Zhang, J. M.; Hoffman, D. M. Resonant Interband Raman-Scattering in Metals and Semimetals. *Solid State Commun.* **1986**, *57*, 567–570.
48. Kalbac, M.; Reina-Cecco, A.; Farhat, H.; Kong, J.; Kavan, L.; Dresselhaus, M. S. The Influence of Strong Electron and Hole Doping on the Raman Intensity of Chemical Vapor-Deposition Graphene. *ACS Nano* **2010**, *4*, 6055–6063.
49. There are actually two maxima: one at E_{ex} and one at $E_{ex} - \hbar\omega_G$. With significant broadening, the maximum appears between these two peaks.
50. Basko, D. M. Calculation of the Raman G Peak Intensity in Monolayer Graphene: Role of Ward Identities. *New J. Phys.* **2009**, *11*, 095011.
51. Ando, T.; Koshino, M. Field Effects on Optical Phonons in Bilayer Graphene. *J. Phys. Soc. Jpn.* **2009**, *78*, 034709.
52. Gava, P.; Lazzeri, M.; Saitta, A. M.; Mauri, F. Probing the Electrostatic Environment of Bilayer Graphene Using Raman Spectra. *Phys. Rev. B* **2009**, *80*, 155422.
53. Malard, L. M.; Elias, D. C.; Alves, E. S.; Pimenta, M. A. Observation of Distinct Electron−Phonon Couplings in Gated Bilayer Graphene. *Phys. Rev. Lett.* **2008**, *101*, 257401.
54. Yan, J.; Villarson, T.; Henriksen, E. A.; Kim, P.; Pinczuk, A. Optical Phonon Mixing in Bilayer Graphene with a Broken Inversion Symmetry. *Phys. Rev. B* **2009**, *80*, 241417.
55. Koshino, M. Interlayer Screening Effect in Graphene Multilayers with ABA and ABC Stacking. *Phys. Rev. B* **2010**, *81*, 125304.
56. Yoon, D.; Moon, H.; Son, Y. W.; Choi, J. S.; Park, B. H.; Cha, Y. H.; Kim, Y. D.; Cheong, H. Interference Effect on Raman Spectrum of Graphene on SiO_2/Si. *Phys. Rev. B* **2009**, *80*, 125422.
57. Ohta, T.; Bostwick, A.; McChesney, J. L.; Seyller, T.; Horn, K.; Rotenberg, E. Interlayer Interaction and Electronic Screening in Multilayer Graphene Investigated with Angle-Resolved Photoemission Spectroscopy. *Phys. Rev. Lett.* **2007**, *98*, 206802.
58. Guinea, F. Charge Distribution and Screening in Layered Graphene Systems. *Phys. Rev. B* **2007**, *75*, 235433.
59. Zhou, S. Y.; Siegel, D. A.; Fedorov, A. V.; Lanzara, A. Metal to Insulator Transition in Epitaxial Graphene Induced by Molecular Doping. *Phys. Rev. Lett.* **2008**, 101.
60. Moreh, R.; Finkelstein, Y.; Shechter, H. NO_2 Adsorption on Grafoil between 297 and 12 K. *Phys. Rev. B* **1996**, *53*, 16006–16012.
61. Sjovall, P.; So, S. K.; Kasemo, B.; Franchy, R.; Ho, W. NO_2 Adsorption on Graphite at 90-K. *Chem. Phys. Lett.* **1990**, *172*, 125–130.

62. Ulbricht, H.; Zacharia, R.; Cindir, N.; Hertel, T. Thermal Desorption of Gases and Solvents from Graphite and Carbon Nanotube Surfaces. *Carbon* **2006**, *44*, 2931–2942.
63. Leenaerts, O.; Partoens, B.; Peeters, F. M. Adsorption of H_2O, NH_3, CO, NO_2, and NO on Graphene: A First-Principles Study. *Phys. Rev. B* **2008**, *77*, 125416.
64. Locatelli, A.; Knox, K. R.; Cvetko, D.; Mentes, T. O.; Nino, M. A.; Wang, S. C.; Yilmaz, M. B.; Kim, P.; Osgood, R. M.; Morgante, A. Corrugation in Exfoliated Graphene: An Electron Microscopy and Diffraction Study. *ACS Nano* **2010**, *4*, 4879–4889.
65. Horng, J.; Chen, C. F.; Geng, B. S.; Girit, C.; Zhang, Y. B.; Hao, Z.; Bechtel, H. A.; Martin, M.; Zettl, A.; Crommie, M. F.; *et al.* Drude Conductivity of Dirac Fermions in Graphene. *Phys. Rev. B* **2011**, *83*, 165113.
66. Li, Z. Q.; Henriksen, E. A.; Jiang, Z.; Hao, Z.; Martin, M. C.; Kim, P.; Stormer, H. L.; Basov, D. N. Dirac Charge Dynamics in Graphene by Infrared Spectroscopy. *Nat. Phys.* **2008**, *4*, 532–535.
67. Jung, N.; Crowther, A. C.; Kim, N.; Kim, P.; Brus, L. Raman Enhancement on Graphene: Adsorbed and Intercalated Molecular Species. *ACS Nano* **2010**, *4*, 7005–7013.
68. Kostecki, R.; Pollak, E.; Geng, B. S.; Jeon, K. J.; Lucas, I. T.; Richardson, T. J.; Wang, F. The Interaction of Li(+) with Single-Layer and Few-Layer Graphene. *Nano Lett.* **2010**, *10*, 3386–3388.
69. Brus, L. Commentary: Carbon Nanotubes, Cdse Nanocrystals, and Electron−Electron Interaction. *Nano Lett.* **2010**, *10*, 363–365.
70. Zhao, L.; He, R.; Rim, K. T.; Schiros, T.; Kim, K. S.; Zhou, H.; Gutierrez, C.; Chockalingam, S. P.; Arguello, C. J.; Palova, L.; *et al.* Visualizing Individual Nitrogen Dopants in Monolayer Graphene. *Science* **2011**, *333*, 999–1003.
71. Hebard, A. F.; Tongay, S.; Hwang, J.; Tanner, D. B.; Pal, H. K.; Maslov, D. Supermetallic Conductivity in Bromine-Intercalated Graphite. *Phys. Rev. B* **2010**, *81*, 115428.
72. Hwang, J.; Carbotte, J. P.; Tongay, S.; Hebard, A. F.; Tanner, D. B. Ultrapure Multilayer Graphene in Bromine-Intercalated Graphite. *Phys. Rev. B* **2011**, *84*, 041410.
73. Dingle, R.; Stormer, H. L.; Gossard, A. C.; Wiegmann, W. Electron Mobilities in Modulation-Doped Semiconductor Heterojunction Superlattices. *Appl. Phys. Lett.* **1978**, *33*, 665–667.
74. Paul, D. J. Silicon−Germanium Strained Layer Materials in Microelectronics. *Adv. Mater.* **1999**, *11*, 191–204.
75. Stormer, H. L. Novel Physics in Two Dimensions with Modulation-Doped Heterostructures. *Surf. Sci.* **1984**, *142*, 130–146.
76. Harwood, M. H.; Jones, R. L. Temperature-Dependent Ultraviolet-Visible Absorption Cross-Sections of NO_2 and N_2O_4-Low-Temperature Measurements of the Equilibrium-Constant for $2NO_2$ Reversible-Arrow-N_2O_4. *J. Geophys. Res., [Atmos.]* **1994**, *99*, 22955–22964.